

**Atomic mechanisms and diffusion anisotropy of Cu tetramers on Cu(111)**J. Ferrón,<sup>1,\*</sup> R. Miranda,<sup>2</sup> and J. J. de Miguel<sup>3</sup><sup>1</sup>*Instituto de Física del Litoral and Departamento de Materiales FIQ, CONICET and Universidad Nacional del Litoral, 3000 Santa Fe, Argentina*<sup>2</sup>*Departamento de Física de la Materia Condensada and Condensed Matter Physics Center (IFIMAC), Universidad Autónoma de Madrid, and Madrid Institute of Advanced Studies - Nanoscience (IMDEA-Nanociencia), Cantoblanco, 28049 Madrid, Spain*<sup>3</sup>*Departamento de Física de la Materia Condensada and Condensed Matter Physics Center (IFIMAC) and Instituto de Ciencia de Materiales “Nicolás Cabrera”, Universidad Autónoma de Madrid, Cantoblanco, 28049 Madrid, Spain*

(Received 8 May 2014; revised manuscript received 29 August 2014; published 22 September 2014)

The surface diffusion of compact Cu tetramers on Cu(111) has been studied at the atomic scale by means of molecular dynamics simulations using embedded atom interatomic potentials. The Cu clusters diffuse by several different mechanisms; all of them have the common trait of involving concerted displacements of at least some of the atoms forming the island. The anisotropy in the rhombus shape of the Cu tetramers and the different activation energies of the translational and rotational jumps result in highly anisotropic diffusion, with a transition from practically one-dimensional motion at low temperature to nearly isotropical two-dimensional random walk at high temperature. The use of molecular dynamics allows us to also determine the preexponential factors for each jump mechanism, from which analysis we can obtain some insight into their basic nature and the relationships between them.

DOI: [10.1103/PhysRevB.90.125437](https://doi.org/10.1103/PhysRevB.90.125437)

PACS number(s): 68.35.Fx, 68.47.De, 71.15.Pd, 82.20.Db

**I. INTRODUCTION**

Despite having been an active area of research for a long time [1–3], surface atomic diffusion keeps offering abundant subjects of interest for further exploration. As both theoretical and experimental tools gain in accuracy and sensitivity, a wealth of novel atomic-scale phenomena are coming to light that can have a significant impact on our understanding of this rich phenomenon. Many different examples can be found in the recent literature: besides the commonly assumed hopping mechanism for monomer diffusion, the atomic exchange was first predicted theoretically [4] and then observed in field ion microscopy (FIM) experiments [5,6]. Another of the basic postulates of classical diffusion theory, namely that the atomic trajectories are made up of individual nearest-neighbor hops, has also been proven too restrictive: longer jumps occur frequently [7–11] and have a sizable influence on nucleation and the growth mode of overlayers [12]. Finally, it has also been shown that in many cases the atomic jump directions are not statistically random, but rather result from complicated correlations involving the diffusing adatom(s) plus several neighbors, both within the overlayer and in the substrate [13,14].

The interest in surface diffusion originates mainly from the many phenomena that are controlled or influenced by mass transport; these include epitaxial growth, chemical reactions at surfaces, catalysis, phase transitions, microelectronics, nanofabrication, etc. [15,16]. With respect to nucleation and growth, most atomistic studies have traditionally dealt with single adatoms. Moreover, a rather common mistake is to confuse the *critical nucleus size* (i.e., the minimum number of atoms required to form a stable island that will, in principle, not dissociate) and the minimum size of islands that can be considered immobile on the surface [17]. In some cases, small

clusters such as dimers or trimers can be as mobile or even more mobile than single monomers [18], thanks to complex, concerted motion processes. In any case, it is nowadays clear that the mobility of small two-dimensional (2D) islands, particularly on close-packed surfaces, must also be taken into account [19–22].

When dealing with island diffusion, one of the fundamental problems is the determination of the atomic mechanisms of motion. From the experimental point of view, most of the original data were obtained by means of field ion microscopy [23–25]. Although it provides atomic resolution, FIM cannot offer images in real time and therefore the diffusion pathways must be inferred from an analysis of the displacements recorded in static snapshots separated by fixed time intervals [1,26]. The actual atomic trajectories, on the other hand, can be easily derived from numerical simulations. With the recent spectacular increase in computational power together with the development of effective potentials such as those provided by the embedded atom method (EAM) [27–29] which allow one to efficiently and accurately reproduce the atomic interactions, it has now become possible to simulate complex processes involving large numbers of atoms during realistic time intervals. Molecular dynamics (MD) is a particularly attractive method because the atomic displacements are calculated in real time, thus enabling us to not only detect the different diffusion mechanisms and determine their activation energies but also their individual prefactors, which contain information about the dynamical particularities of each process.

The earliest FIM studies, also supported by calculations, concluded that island motion in general required the partial detachment of a border atom followed by its diffusion along the island edge to a different position, thereby provoking a displacement of the cluster's center of mass [1,5,24,30,31]. Nevertheless, it soon became clear, mainly thanks to theoretical and simulation studies, that the smallest islands (below approximately 10–15 atoms) diffuse preferentially by coordinated processes involving several or all of the atoms in

\*jferron@intec.unl.edu.ar

the cluster [32–36]. It seems well established now that there exist two regimes for the diffusion of 2D islands as a function of their size: while the large ones move by displacements of atoms around their periphery with a roughly constant effective activation energy [31,37,38], for small islands this energy typically shows an increasing trend with island size [5,32,39,40] that reflects the growing difficulty in achieving the concerted motion of all the atoms in the cluster. Some oscillations that are related to the existence of *magic* island sizes of particular stability [3,5,17,41–44] are frequently observed superimposed on this general increasing trend; for instance, compact tetramers are usually more mobile on fcc-(111) surfaces than trimers [17,22,24,42,45]. The crossover between those two regimes appears when the limiting process for edge diffusion, namely the detachment of an adatom from a kink or corner site, becomes energetically favorable with respect to the energy required to move the island by any of the collective mechanisms [38]. For even larger sizes, other mechanisms may come into play, such as vacancy diffusion inside the islands [46]. Finally, in heteroepitaxial systems where lattice mismatch also participates in the total energy, the formation of misfit dislocations within the islands represents another significant contribution to consider [47,48].

In this work, we have studied the diffusion of a Cu tetramer on Cu(111) with a special focus on the different mechanisms that result in island rotation. The tetramer is particularly interesting for several reasons. In the first place, the compact tetramer on a fcc-(111) surface is intrinsically anisotropic, having the shape of a rhombus with a long and a short diagonal. As we shall see, this fact translates into a predominantly one-dimensional motion at low temperature that transforms to the usual, two-dimensional random walk at higher temperatures. Diffusion anisotropy has a strong influence in nucleation, growth, and the formation and morphology of nanostructures [3,34,49]. The tetramer is still a reasonably simple object yet complex enough to have already shown a variety of diffusion mechanisms in previous studies [17,33,40,42,45,50–53]. Furthermore, the tetramer is also one of the magic sizes that show an anomalously low activation energy, being one atom larger than the more morphologically stable trimer [22,54]. Its relatively unstable configuration facilitates the structural distortions and enables several different diffusion mechanisms that we describe here. By using molecular dynamics simulations over a broad range of temperatures, we can identify all the different atomistic processes in an unbiased manner and determine their individual activation energies and prefactors. This is achieved from Arrhenius analyses of the frequencies of occurrence of each one of them. This procedure is the safest one because it simply lets the system evolve freely, responding to the interactions between the constituent atoms without imposing any restrictions on the atomic trajectories or limiting the catalog of different mechanisms to consider. The analysis of the activation energies and the prefactors allows us to draw some conclusions about the nature of each process and the relevance of correlated atomic displacements.

## II. METHODOLOGY

The simulations were carried out using the XMD package [55]. The atomic interactions were accounted for by means

of empiric EAM potentials [56]. The Cu(111) substrate was simulated by a slab of 12 layers of 240 atoms each, with vacuum on both surfaces and periodic boundary conditions in all directions. Before each run, the sample was fully relaxed to minimize its energy, except for the three deepest atomic layers that were kept frozen to simulate the bulk. The four Cu atoms forming the cluster were deposited initially on ideal fcc sites already forming a compact rhombus but slightly above their expected equilibrium heights. All atomic positions were then allowed to equilibrate and the whole system was thermalized for 50 ps before starting to record the cluster displacements. The simulations were carried out at constant temperature, using an algorithm that rescales all atomic velocities in order to match the appropriate Maxwell-Boltzmann distribution for the specified temperature. Since we intended to observe and compare diverse atomistic processes taking place at several temperatures and on different time scales, the same integration time step of 1 fs was used in all simulations. The atomic coordinates were stored at intervals of 40 fs to allow us to follow the atomic trajectories with sufficient precision [10]. These coordinates have been used to produce movies that graphically display all the different cluster motion events, facilitating their identification and description by simple inspection. See Supplemental Material [57] for some sample movies showing short simulations at 270, 390, and 600 K. The duration of the runs conducted at each temperature was prolonged until a representative number of jumps was accumulated—at least for the temperatures at which the tetramer is reasonably mobile—with a minimum of 10 ns at the highest temperatures, which display the largest jump frequencies and thus the best statistics.

Tetramer displacements were detected automatically by an algorithm that calculates at each step the in-plane distance between the atoms forming the cluster and the nearest adsorption sites on the substrate. A jump was considered accomplished when at least some of the atoms were occupying positions different from the previous stable ones and the tetramer's center of mass had moved from one surface unit cell to another. We also kept track of the tetramer's orientation by continuously monitoring the alignment of its long and short diagonals. In view of the sixfold symmetry of the substrate, a change of more than 30 degrees in the direction of these axes was taken as the signal of a cluster rotation. In the figures throughout this paper and also in the movies available as Supplemental Material in the online version [57], the individual atoms forming the Cu<sub>4</sub> cluster are depicted in different colors to facilitate their identification. For easier referral, they have also been numbered 1 through 4 in the figures. The tetramer maintained a compact shape at all times during the simulations and at all temperatures explored, except during the rotations executed by the atom swap mechanism, described in Sec. III D. For all types of events, a time threshold of 0.8 ps was established: all jumps or rotations resulting in shorter residence times at the new position were considered fluctuations and discarded. The choice of this value was initially motivated by our previous work on the diffusion of Cu monomers on Cu(111) [10], where we found that the fastest diffusion processes for single atoms took at least  $\approx 0.4$  ps. As it will be shown in Sec. III below, all of the different types of jumps and rotations of the tetramer that we have observed in this work take place over time intervals

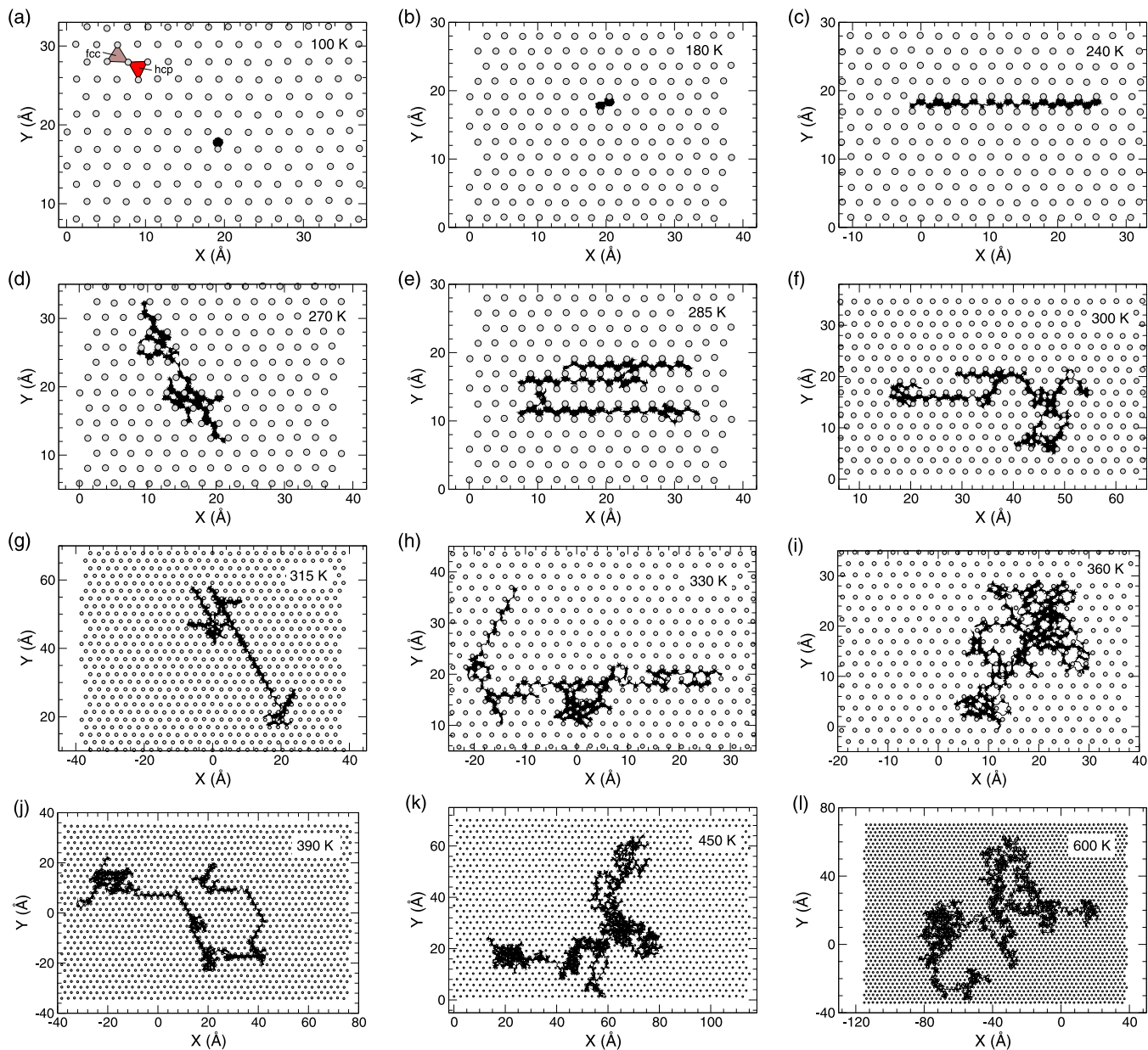


FIG. 1. (Color online) Center-of-mass trajectories resulting from simulations at different temperatures: (a) 100, (b) 180, (c) 240, (d) 270, (e) 285, (f) 300, (g) 315, (h) 330, (i) 360, (j) 390, (k) 450, (l) 600 K. Adsorption sites corresponding to the fcc and hcp stacking sequences are shown in (a).

of the order of 1 ps or longer, thus confirming the validity of our present criterion.

### III. RESULTS

Figure 1 displays the trajectories of the tetramer’s center of mass obtained at all the temperatures examined in our study. Below 200 K, the cluster is very scarcely mobile: a single jump was observed at 180 K after 9.2 ns of simulation, and none at 100 K. The tetramer’s mobility progressively increases with raising temperature describing first a quasi-one-dimensional zigzag path oriented parallel to the tetramer’s short diagonal and made up of nearest-neighbor jumps alternating between adjacent fcc and hcp adsorption sites. At 270 K, some changes

of direction start to appear; these events are associated with cluster rotations, i.e., atomic jumps that change the orientation of the tetramer’s axes. After each of these jumps, the linear displacements continue parallel to the new short diagonal, so that the net displacement is always parallel to this direction, whatever its macroscopic alignment with respect to the surface.

The frequency of rotations increases continuously with temperature, with different mechanisms appearing gradually, which will be discussed below. Only above  $\sim 450$  K do the tetramer’s trajectories start to resemble a truly two-dimensional random walk over the surface. Finally, at 600 K, the atomic displacements are no longer restricted to the threefold hollow adsorption sites, indicating that the cluster is performing a flight above the surface.

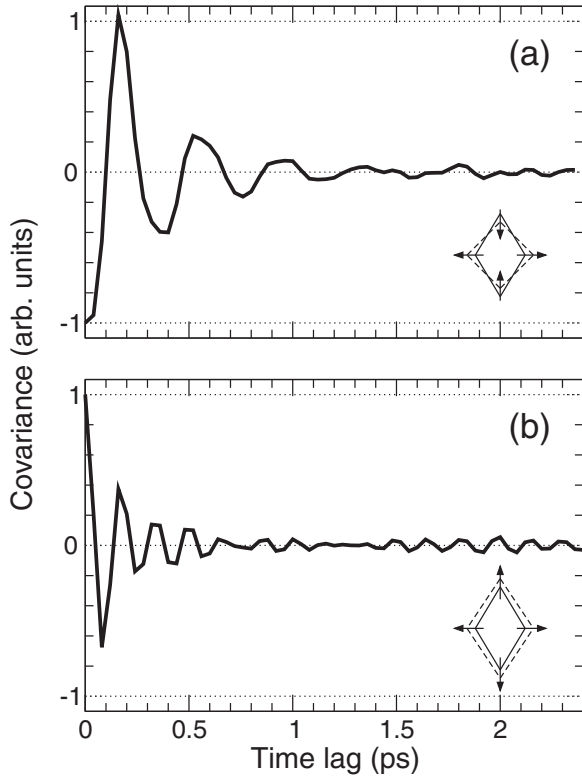


FIG. 2. Main vibrational modes of the Cu tetramer, identified from the analysis of the atomic displacements as a function of time. (a) Bending mode, consisting of the compression of the tetramer's long diagonal and the stretching of the short one. (b) Breathing mode, in which the tetramer's area pulsates as a function of time.

### A. Cluster vibrations and thermal evolution of the aspect ratio

The cluster vibrations play an important role in the different migration processes and we have characterized them by monitoring the lengths of the tetramer's long and short diagonals; the aspect ratio  $R$  is defined as the quotient of these two magnitudes and gives us a measure of the deformation of the island with respect to its ideal rhombus shape, for which  $R$  amounts to  $2 \cos(\pi/6) = 1.732$ .

Our simulations show how the four atoms in the tetramer are permanently vibrating in their adsorption sites. An inspection of the time evolution of the long- and short-diagonal lengths reveals the correlations between them; it turns out that the bending mode is the dominant vibrational mechanism. Figure 2(a) shows the normalized covariance of the two rhombus diagonals. The value of  $-1$  at zero time shift between them indicates that the two magnitudes are oscillating in phase opposition: when one of them is maximum, the other one is at a minimum, and vice versa. This vibrational mode has a frequency of  $(2.63 \pm 0.03) \times 10^{12}$  Hz as determined from the period of the covariance oscillations [53,58–62]. A breathing mode of the tetramer can also be detected: in this case, we examine the product of the lengths of both diagonals, a quantity that is proportional to the island's area. The self-covariance of this magnitude is presented in Fig. 2(b) and the oscillation period in this case yields a frequency of  $(6.00 \pm 0.03) \times 10^{12}$  Hz.

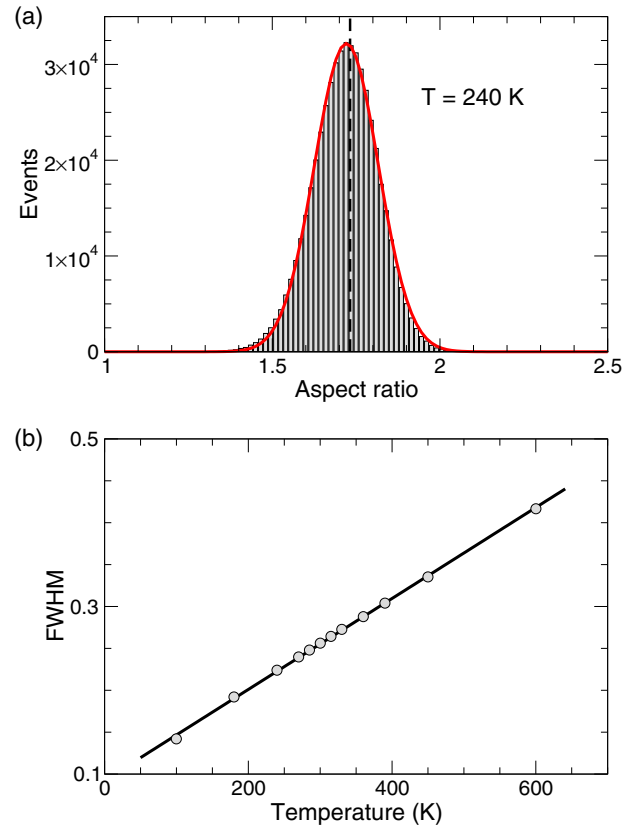


FIG. 3. (Color online) (a) Histogram of the values taken by the tetramer's aspect ratio  $R$  during the simulation at 240 K. The solid line is a Gaussian fit to the data, and the dashed line marks the nominal value of 1.732. (b) Evolution of the FWHM of the histograms of aspect ratios at the different temperatures of the simulations. The solid line is a linear fit to the data.

Other vibrations and fluctuations of the tetramer shape are more difficult to identify. However, the magnitude of those distortions can be quantitatively characterized by means of the aspect ratio  $R$ . As an example, Fig. 3(a) depicts a histogram of the values taken by this parameter at 240 K. At this temperature, the distribution appears centered slightly below the nominal value of 1.732 (marked by the vertical dashed line), and it can be nicely fitted with a Gaussian curve, revealing that the probability of each deformation is inversely proportional to its deviation from the equilibrium cluster shape. Similar fits can be obtained for all the other temperatures studied; their full width at half maximum (FWHM), which measures the magnitude of the shape fluctuations in each case, follows a strict linear dependence, as shown in Fig. 3(b), indicating that with increasing thermal energy the tetramer progressively occupies higher states above the sample's potential energy landscape, thereby becoming more and more decoupled from it. Thus, the amplitude and frequency of its distortions with respect to the ideal shape dictated by the fcc surface template also grow correspondingly. Given the low corrugation of the Cu(111) face, the range of thermal energies explored in our calculations covers a large fraction of the diffusion barrier ( $\approx 40$  meV for Cu monomers [61–64]) and hence one can

TABLE I. Activation energies and prefactors for each of the different diffusive jumps of the Cu tetramer, as derived from the Arrhenius fits of Fig. 9.

Type of jump	Prefactor $\nu_{\text{eff}}$ (THz)	Activation energy $E_a$ (eV)
Short diagonal glide	$2.0(\times 2.0^{\pm 1})$	$0.15 \pm 0.02$
Shearing rotation	$1.5(\times 1.3^{\pm 1})$	$0.20 \pm 0.01$
Concerted rotation	$4.1(\times 1.4^{\pm 1})$	$0.29 \pm 0.02$
Long diagonal glide	$0.5(\times 1.5^{\pm 1})$	$0.20 \pm 0.02$
Atom swap	$13.1(\times 2.2^{\pm 1})$	$0.37 \pm 0.03$

expect to observe significant shape differences between the lowest and the highest temperatures studied.

**B. Dislocation-based mechanisms**

In the following, we shall describe at the atomic level the different types of jumps that show up in our simulations and that produce the trajectories depicted in Fig. 1. We start with two diffusion processes that involve the appearance of a dislocation that partially separates the tetramer in two halves and creates a shearing deformation from its ideal rhombus shape. Both of them are probably related to the fundamental vibrational bending mode described above.

**1. Short-diagonal glide**

The diffusion event with the lowest energy that we observe (see Table I) is the concerted glide or reptation parallel to the tetramer’s short diagonal that conforms the linear paths, such as the one that can be observed at 240 K in Fig. 1(c). The displacement mechanism is schematically depicted in Fig. 4(a) as a sequence of snapshots taken from an actual simulation. These jumps are accomplished in a concerted fashion, triggered by two adjacent atoms (3 and 4 in this example) that initiate the displacement across the nearby bridge sites causing a slight shear distortion of the diamond-shaped island; the other

two atoms of the tetramer follow afterwards, completing the crossing. The whole process takes in general more than 1 ps in our simulations (about 3 ps in this particular example), thus supporting our choice of 0.8 ps for the threshold to discriminate stable jumps. This mechanism was first proposed by Wang and Ehrlich based on their groundbreaking FIM experiments on Ir<sub>4</sub>/Ir(111) [24], who even succeeded in imaging one tetramer frozen at the transition stage, and confirmed later by numerous reports [17,33,40,42,45,53,65,66]. It is remarkable that from the three possible bridge crossings existing at each adsorption site, the one situated along the tetramer’s long diagonal is systematically avoided in these displacements. This latter jump, which has also shown up in various other studies of jump energetics [17,40,42,45,53], only appears at the highest temperatures explored in our study. In fact, it is the least abundant event in our simulations and, most significantly, it does not involve any dislocation or shearing of the tetramer, but rather takes place as a concerted motion of the cluster as a whole. For this reason, it will be discussed in the next section, together with the concerted rotation. To characterize the degree of atomic correlation in these jumps, we also resort to the statistical analysis of the tetramer’s aspect ratio. Figure 4(b) shows the histogram of values of  $R$  at 240 K (a temperature where only short-diagonal jumps occur) restricted to short intervals of time centered around each crossing. In the same graph, we also plot with a solid red line the distribution of aspect ratios during the rest of the time in the simulation, when no jumps are completed. Although the two curves are very similar, one can observe a slight increase in the frequency of lower  $R$  values during the crossings, revealing the distortion of the tetramer caused by the atoms that initiate the jump.

**2. Rhombus shearing rotation**

The first changes in the orientation of the tetramer appear at 270 K. The cluster reorientation proceeds by a shearing deformation of the rhombus, as illustrated in Fig. 5(a): again in this case, the process is initiated by two adjacent atoms (2 and 3 in this example), followed by the other two that

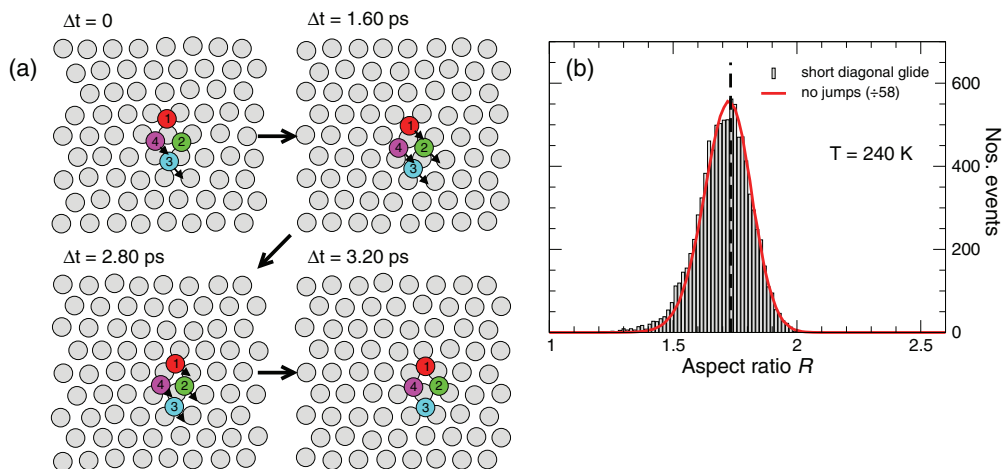


FIG. 4. (Color online) (a) Series of MD simulation snapshots illustrating the coordinated atomic displacements that result in a translational jump of the tetramer by the short diagonal glide mechanism. (b) Distribution of values of the aspect ratio  $R$  during short diagonal glide jumps at 240 K. The solid red line reproduces the values of  $R$  at the same temperature during the time when no jumps are taking place; this curve has been rescaled to compare it with the data for the jump stage.

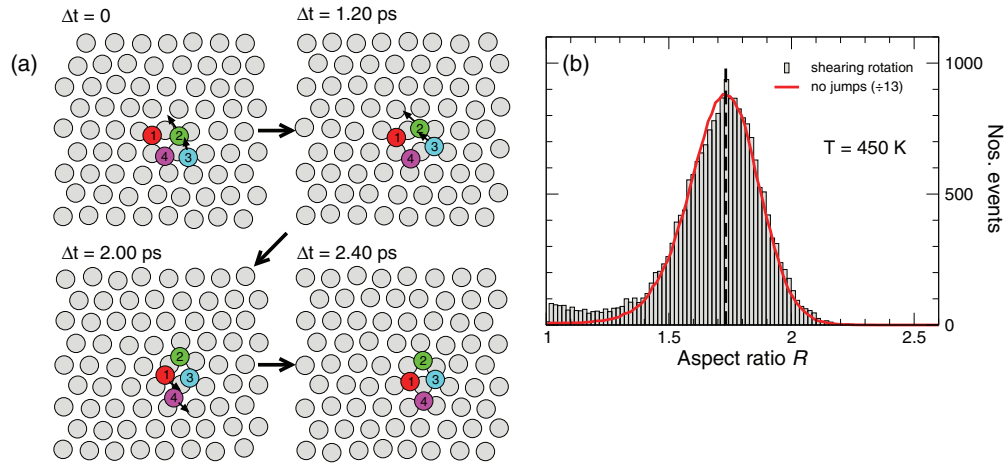


FIG. 5. (Color online) (a) MD simulation snapshots illustrating the atomic displacements resulting in a tetramer’s rotation by the shearing mechanism. (b) Distribution of values of the aspect ratio  $R$  during the shearing rotations observed at 450 K. The solid red line displays the values of  $R$  at the same temperature during the time when no jumps are taking place; this curve has been rescaled to compare it with the data for the jump stage.

move in the opposite direction. This mechanism was also first identified by Wang and Ehrlich [24] and it is characterized by the swap of the tetramer’s diagonals: the former short one becomes the long one after the rotation, and vice versa. The sequence of atoms around the tetramer (1-2-3-4), though, remains unaltered. This process is thus clearly reflected in the variation of the aspect ratio presented in Fig. 5(b). The data used to construct this graph have been extracted from the simulations carried out at 450 K, which present a reasonable number of jumps of this type to ensure good statistics. The tail of the histogram that extends down to  $R = 1$  shows how the cluster progressively deforms until at the transition point both diagonals have the same length. The graph is truncated at this value because, due to our definition of the aspect ratio, once the two axes have exchanged roles,  $R$  starts to increase again toward the equilibrium value with the tetramer’s axes pointing along their new orientations. For comparison, the histogram is plotted in this figure together with the aspect ratios obtained

at the same temperature, but during the time when no jumps are taking place. This one is depicted with a solid red line in the figure.

### C. Concerted jump mechanisms

Next we deal with another set of diffusion jumps characterized by the simultaneous translation of all the atoms constituting the cluster, with very little or no accompanying distortion of the rhombus shape.

#### 1. Concerted rotation

Starting at 315 K, we observe tetramer rotations that do not correspond to the pattern described above for the shearing deformation. In this type of jump, the tetramer executes a concerted rotation with the atoms simultaneously crossing a nearby bridge site, as schematically depicted in Fig. 6(a). This process can be easily distinguished from the previous one

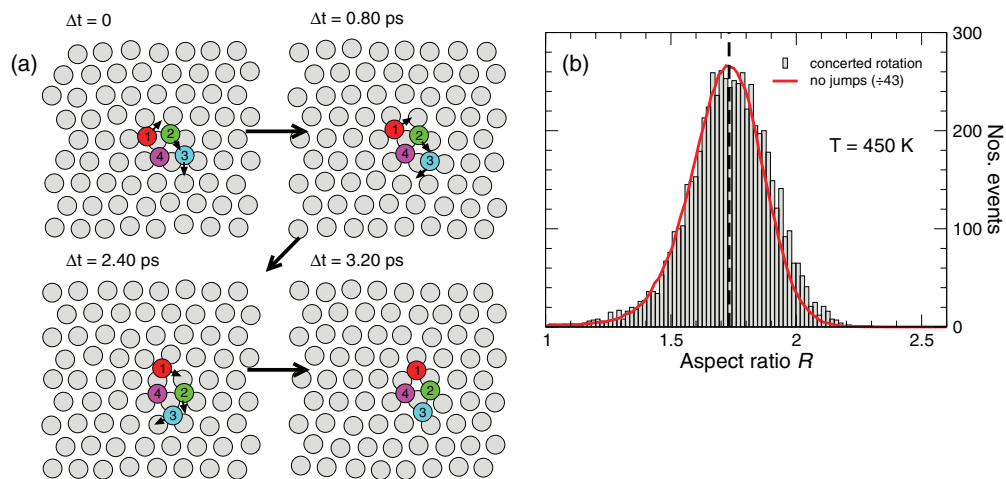


FIG. 6. (Color online) (a) MD simulation snapshots describing the concerted rotation mechanism of the Cu tetramer. (b) Distribution of values of the aspect ratio  $R$  during the concerted rotations observed at 450 K. The solid red line gives the values of  $R$  at the same temperature during the time when no jumps are taking place; this curve has been rescaled to compare it with the data for the jump stage.

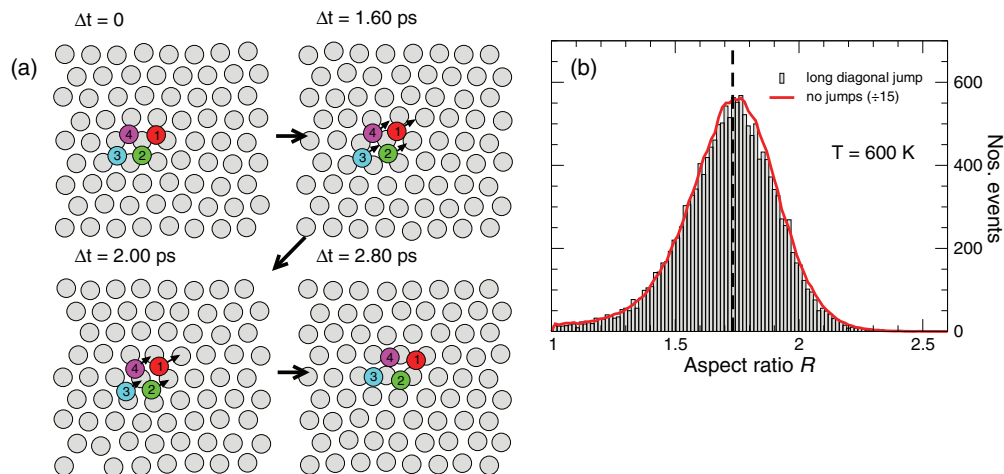


FIG. 7. (Color online) (a) MD simulation snapshots illustrating the long diagonal glide mechanism of translational motion. (b) Distribution of values of the aspect ratio  $R$  during the long diagonal glide jumps observed at 600 K. The solid red line summarizes all the values of  $R$  recorded at the same temperature; this curve has been rescaled to compare it with the data for the jump stage.

because the long and short diagonals do not change, and the atoms situated at the corners remain the same after the turn.

A close inspection of the evolution of the aspect ratio presented in Fig. 6(b) offers interesting clues about the details of these processes. This analysis has been carried out also at 450 K and the comparison of the data corresponding to the transition stages with the distribution of values of  $R$  during the rest of the simulation shows that the histogram of aspect ratios during these concerted rotations is shifted to slightly higher values (i.e., more elongated shape), suggesting that at this stage the cluster is floating at a higher-energy state with respect to the sample's potential-energy surface and thus the atoms occupying the tip positions at both ends of the long diagonal have a higher probability to stretch away from the tetramer's center of mass. In this way, this type of jump can be considered as a precursor of the last jump mechanism that will be discussed in this paper, namely, the *atom swap*.

## 2. Long-diagonal glide

From 390 K upwards, we also observe a gradually increasing number of translational jumps in which the tetramer moves in the direction parallel to its long diagonal. This type of displacement, with all the atoms in the cluster moving simultaneously in the same direction, has been known in general in the literature as “concerted glides.” In this work, we have preferred to call them long-diagonal glides for two reasons: (i) This nomenclature has already been introduced in previous works dealing with diffusing tetramers on fcc(111) surfaces [40,53], and (ii) we find it more descriptive and allowing for an easier distinction with respect to the short-diagonal glide mechanism described in Sec. III B 1. The process is depicted in Fig. 7(a): all four atoms simultaneously cross the corresponding bridge sites without apparent distortion of the cluster's diamond shape. This observation is confirmed by the analysis of the aspect ratio at 600 K, which is presented in Fig. 7(b). Here we see how the distribution of values of  $R$  restricted to the time intervals when the long-diagonal glide jumps are taking place coincides exactly with the global one, implying that the successful displacements do not involve

any particular distortion of the atoms forming the tetramer. From this result, we conclude that this diffusion mechanism is essentially different from the short-diagonal glide described above, since the latter involves an initial motion by a part of the cluster with the rest of it following afterwards.

It is also noteworthy that both curves in Fig. 7(b) are clearly shifted towards values of  $R > 1.732$ , following the tendency already detected in Fig. 6(b) at 450 K. Thus, at elevated temperatures, the tetramer shape and its interatomic distances are dominated by the effect of the thermal fluctuations, and the influence of the surface atomic structure becomes progressively weaker. In fact, at 600 K, we observe how the trajectory followed by the diffusing tetramer is no longer restricted to a sequence of alternating fcc/hcp threefold adsorption sites and numerous passages through atop positions can be detected.

## D. Atom swap

The last atomic-scale mechanism capable of inducing a reorientation of the tetramer that we have been able to identify in our simulations involves a relatively complex internal reorganization of the atoms forming the cluster, as shown in Fig. 8. In this process, one of the atoms occupying the ends of the long diagonal (number 1 in this case) nearly detaches from the rest, which form a compact trimer. The transformation then proceeds in a concerted manner, with the diffusing atom turning around the nearby corner of the trimer while at the same time this latter performs a rotation in the opposite sense. After that, the fourth atom reattaches to the other three and completes the position exchange. As a result, the atom sequence is altered (1-4-2-3 clockwise in this example) and the orientation of the tetramer's diagonals has changed. It is interesting to notice that this motion mechanism might, under certain circumstances, result in a mere reorganization of the cluster's atomic configuration with no net displacement of its center of mass. Nevertheless, these events have a substantial impact on the tetramer's diffusion since they constitute one of the processes allowing for a change of direction in the otherwise quasi-one-dimensional zigzag paths provoked by the dominating short-axis glide jumps.

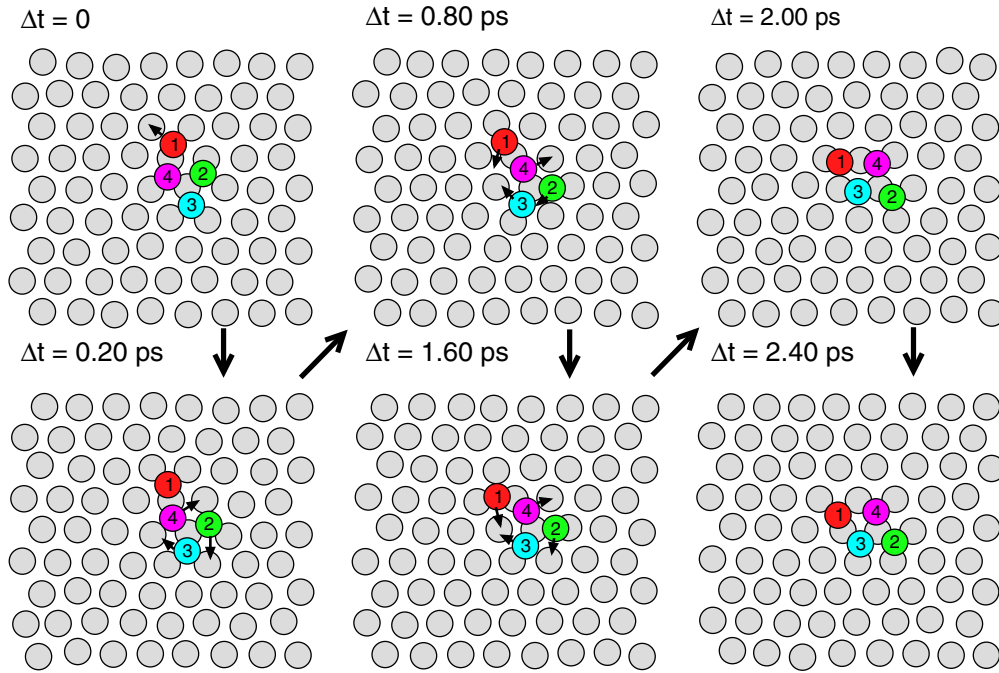


FIG. 8. (Color online) MD simulation snapshots describing the atom swap mechanism of rotation.

This mechanism is obviously a high-energy process due to the need to at least partially break some bonds between the atoms forming the cluster, and as such it is only observed at the highest temperatures in our simulations. Still, it is noteworthy that no instances of cluster dissociation have been observed. No analysis of the aspect ratio has been carried out for this type of jump since the long and short diagonals are not well defined while the rotation is taking place.

### E. Jump energetics

In this section, we study the frequencies of occurrence of each process as a function of temperature. We assume that all of them are thermally activated and fit the data with Arrhenius models (solid lines in the graphs of Fig. 9). The activation energies and prefactors derived from these fits are summarized in Table I.

From this analysis, we find an activation energy  $E_a = 150 \pm 20$  meV for the short-diagonal glide jump [see Fig. 9(a)], in good agreement with the values reported previously by Marinica *et al.* [53] (189 meV for the fcc-to-hcp crossing, and 165 meV for the inverse process) and by Karim *et al.* [40] (167 and 125 meV, respectively). At the highest temperatures of our study (450 and 600 K), the frequency of this type of jump saturates due to the abundance of all the other processes; for this reason, we have excluded these two data points from the fit.

When determining activation energies for specific atomic processes, this method of analysis has the advantage of not imposing any constraints on the atomic trajectories; complex atomic correlations are also included naturally since the system is allowed to evolve freely. The accuracy of the results is then limited only by the quality of the interatomic potentials and by the statistical uncertainty. This is, on the

other hand, the main drawback because long simulation times are required to accumulate sufficient events, especially for the less-frequent processes. In view of the relatively scarce number of events recorded in our simulations, we have not attempted to distinguish between the two senses of the jumps (from fcc to hcp, and vice versa). Our activation energies should thus be taken as an average of both values.

Another advantage of our approach using molecular dynamics is that the simulations are carried out in realistic time scales, thus allowing us to also directly determine the preexponential factor for each process. Since we are dealing with jump frequencies, the parameter derived from our fits is an effective attempt frequency  $\nu_{\text{eff}}$  [62]. For the short-diagonal jumps, we obtain a prefactor of  $2.0(\times 2.0^{\pm 1}) \times 10^{12}$  Hz. This value also coincides within the error bars with those deduced from the analysis of the mean-square displacements of similar clusters in kinetic Monte Carlo simulations:  $1.57 \times 10^{12}$  Hz for Ni tetramers diffusing on Ni(111) [42] and  $1.07 \times 10^{12}$  Hz for Cu tetramers on Cu(111) [40]. Such a coincidence is not surprising because most of the distance covered by the tetramers, at least below 500 K, is due precisely to the short-diagonal glide jumps: the different types of rotations produce a much shorter motion of the cluster's center of mass, and the long-diagonal jumps are scarce.

$\text{Cu}_4$  rotations by the shearing mechanism have also been described by Karim *et al.* [40], who find an activation energy of 230 meV, roughly compatible with our own value of  $200 \pm 10$  meV derived from the data shown in Fig. 9(b). Similarly, 285 and 276 meV are reported for the shearing deformations of Ni tetramers on Ni(111) [42]. No preexponential factors are given in the literature for these specific processes; we find  $1.5(\times 1.3^{\pm 1}) \times 10^{12}$  Hz. This attempt frequency is comparable to that of the short-diagonal glide jumps determined above and both of them are also similar to the frequency of the

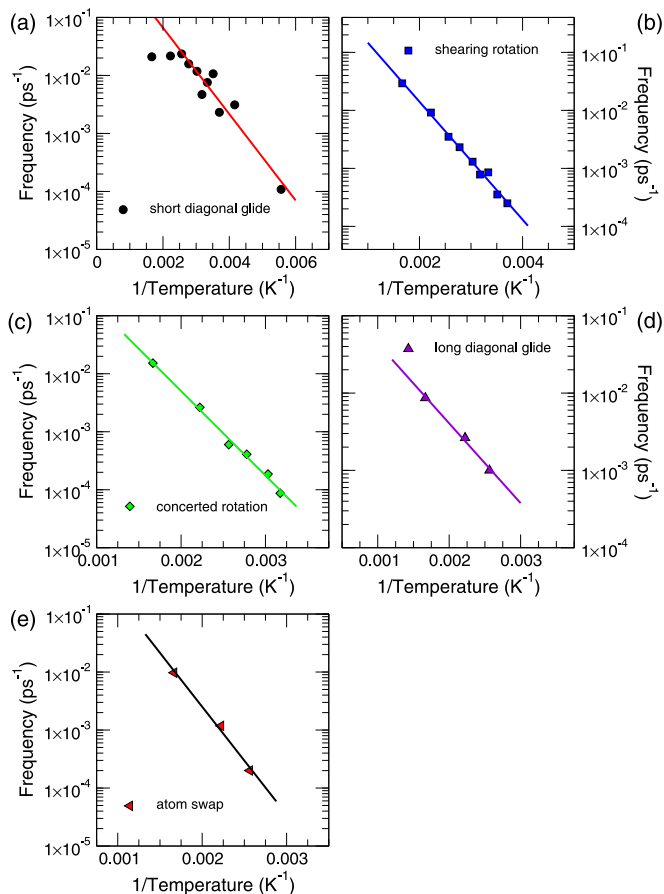


FIG. 9. (Color online) Arrhenius plots representing the frequency of occurrence of the different jump mechanisms as a function of temperature: (a) short diagonal glide, (b) shearing rotation, (c) concerted rotation, (d) long diagonal glide, and (e) atom swap rotation. The straight lines are exponential fits to the data, from which the corresponding prefactors and activation energies are derived and listed in Table I. For the short diagonal glide jumps (a), the two data points at the highest temperatures deviate from the behavior of the rest and have been excluded from the fit.

bending vibrational mode, thus supporting the idea that those two mechanisms somehow derive from that type of cluster vibration. In fact, the schematic cartoons displayed in Figs. 4(a) and 5(a) show that both processes start in the same way, with an initial concerted displacement of two of the tetramer's atoms creating a partial dislocation of the island. The type of jump is defined afterwards, resulting in a short-diagonal glide if the other two atoms follow the first couple with a displacement in the same direction or, conversely, evolving into a shearing rotation if the latter maintain their initial position or even rotate in the opposite sense.

For the concerted rotations, whose data are summarized in Fig. 9(c), we find an activation energy of  $290 \pm 20$  meV and a prefactor of  $4.1(\times 1.4^{\pm 1}) \times 10^{12}$  Hz. The latter is a factor 2–3 times larger than the previous ones, which seems to be a demonstration of the well-known Meyer-Neldel compensation rule [67] and hints that this process has a larger probability than the former. This could be due to the fact that for this mechanism, the cluster rotates rigidly without the need to

adopt for it any specific atomic configuration. The counterpart, which explains the reduced number of events observed is the higher activation energy, suggesting that the simultaneous bridge crossings can only be achieved when the four atoms are occupying a relatively high-energy state within their corresponding potential wells.

The long-diagonal glide mechanism constitutes a special case and is worth some discussion. The corresponding fit is presented in Fig. 9(d). We have only been able to accumulate data for the three highest temperatures. Nevertheless, we find a relatively low activation energy,  $200 \pm 20$  meV, again in reasonable agreement with previous reports: Karim *et al.* [40] find 218 (260) meV for the hcp-to-fcc (fcc-to-hcp) transition, while Marinica *et al.* [53] quote 238 and 262 meV for the same displacements. The preexponential factor calculated here is, however, the lowest of all:  $0.5(\times 1.5^{\pm 1}) \times 10^{12}$  Hz. Since the execution of this jump does not seem to depend on any particular tetramer configuration—as revealed by Fig. 7(b)—the successful attempts must involve correlated atomic movements probably also including the substrate atoms, similarly to what has already been shown for some particular types of jumps of single adatoms [13]. This requirement for a complex, coordinated action from a large number of atoms can thus explain the low value of the prefactor and the correspondingly low probability of these processes [62]. It also allows us to propose that this is a fundamentally different type of process from its apparent counterpart, the short-diagonal glide, since the latter is assisted by the formation of the internal dislocation in the cluster whereas the tetramer remains undistorted during the execution of long-diagonal jumps.

Finally, the highest-energy process observed in our simulations is the atom swap rotation, with an activation energy of  $370 \pm 30$  meV and a prefactor of  $13.1(\times 2.2^{\pm 1}) \times 10^{12}$  Hz as determined from the Arrhenius fit in Fig. 9(e). These values must be taken with some care given the low number of data points available; nevertheless, they are interesting to analyze. The total-energy cost of this rotation involves several contributions, the largest one being the energy required to nearly detach one of the atoms (number 1 in the example of Fig. 8) from the remaining three. This atom then has to perform up to three consecutive bridge crossings, while at the same time the trimer rotates in the opposite direction. The prefactor is substantially larger than all the others reported above, implying that this process has a large likelihood provided that the tetramer acquires the necessary amount of thermal energy from the surrounding medium. Since the rate-limiting step seems to be the partial detachment of the corner atom, we presume that the large activation energy associated with this rotation might be related to the high stability of the compact trimer [17,22,24,32].

### F. Diffusion coefficient

Although the main purpose of this work was to study the different motion mechanisms of the Cu tetramer, we have also attempted to determine its diffusion coefficient by measuring the distance covered by it as a function of time and applying Einstein's relation in two dimensions:  $\langle [r(t) - r(0)]^2 \rangle = 4Dt$  [22]. With the exception of the simulations run at 100 and 180 K, for which the cluster displacement is too short to attempt any statistical analysis, the values of  $D$  obtained by this

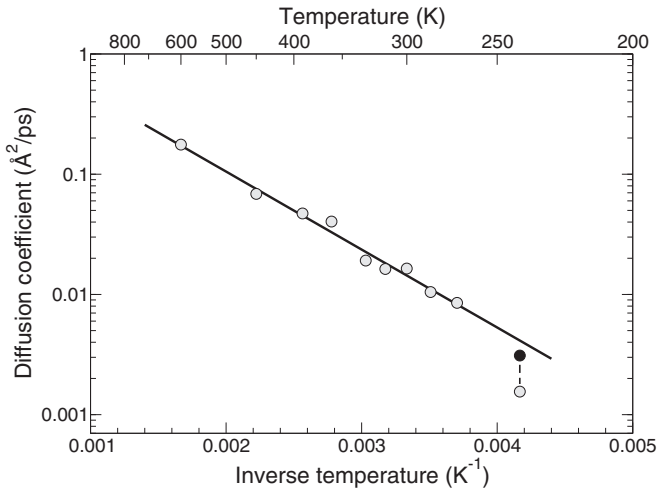


FIG. 10. Diffusion coefficients of the Cu tetramer at different temperatures, derived from the analysis of the quadratic displacement with time, assuming two-dimensional diffusion. The solid line is a fit to the data excluding the data point at 240 K. The black solid circle is the value of the diffusion coefficient at that temperature as calculated for one-dimensional diffusion.

method are plotted in Fig. 10; the solid line is an Arrhenius fit to the high-temperature data. The point at 240 K (circle filled in gray) seems to deviate from the rest and has also been excluded from the fit. All of the other data points yield an effective activation energy of  $E_a = 0.129 \pm 0.006$  eV and a preexponential factor  $D_0 = 2.1(\times 1.2^{\pm 1}) \times 10^{-4}$  cm<sup>2</sup>/s. The activation barrier that we find is significantly smaller than the one reported by Karim *et al.* [40], 212 meV. Nevertheless, it seems reasonable to expect that the global diffusion coefficient derived from the analysis of the net displacement of the tetramer as a function of time should be dominated by the most abundant process, which is the short-diagonal jump. In any case, it is true that our data might be affected by the short distances covered by the island. Our prefactor is also smaller than the one given by these authors that amounts to  $1.5 \times 10^{-3}$  cm<sup>2</sup>/s.

With respect to the anomalous value of  $D$  for 240 K, one should recall that the factor 4 in Einstein's relation appears as a result of assuming a two-dimensional random walk by the moving object. Its use, therefore, does not seem justified for a case of one-dimensional motion such as the one displayed by the Cu tetramer at that temperature. If we take this fact into account and correct the value of  $D$  accordingly, we obtain the data point shaded in black in Fig. 10, in much better agreement with the rest of the data.

#### IV. DISCUSSION

There exists some controversy in the literature regarding the fundamental nature of the different jump mechanisms. In their paper on the diffusion of small Ir clusters on Ir(111) [24], Wang and Ehrlich described both the gliding jump along the short-diagonal direction and the shearing rotation of the tetramers as representing two different outcomes of a same precursor state in which two of the atoms initiate the transition. This view is supported by density-functional theory (DFT)

and EAM-based calculations on the diffusion of Al clusters on Al(111) [17]. On the other hand, theoretical studies of Ni<sub>4</sub> on Ni(111) using EAM potentials [32,33] identified a rigid glide with all four atoms crossing simultaneously through the bridge positions along the short-diagonal direction as the diffusion process with the minimum activation energy. Hamilton *et al.* [33] explicitly distinguished this collective jump from their *dislocation* mechanism, analogous to our short-axis glide with a shear distortion of the island. This point of view is closer to that outlined in other recent reports which also tend to assimilate the two translational gliding jumps along the short and the long diagonals [40,42,53], as opposed to the shear rotations. Our results seem to line up with the original proposal by Wang and Ehrlich: although the difference might appear small, the slight shift of the histogram of aspect ratios in Fig. 4(b) toward smaller values and the similarity of the prefactors suggest a direct relationship between the short-diagonal glide and the shearing rotation. We suggest that the fundamental vibrational mechanism of the Cu<sub>4</sub> tetramer, the bending mode that also reduces the aspect ratio of the island and can result in a shearing distortion of its rhombus shape—see Fig. 2(a)—may lie at the origin of these two processes. The long-axis glide, on the other hand, does not seem to be related to any particular vibrational mode of the system, but rather results from a complicated coordination of multiple atomic displacements, analogous to the concerted rotation. In any case, it is conceivable that fine details in the vibrational characteristics of the different materials and even crystal faces, or the binding strength between the atoms forming the island, might have a significant influence on the diffusion mechanisms, thus explaining the somewhat contradictory reports that have appeared so far.

In their work, Wang and Ehrlich [24] also noted that the short-diagonal glide cannot continue in a straight line since after the first jump the continuation would force the tetramer's atoms to cross through atop positions. For this reason, they proposed a translation mechanism for long-distance displacements consisting of the partial detachment of two of the tetramer's atoms with the other two following them. Such a process has not been observed in our simulations, which rather show that the linear, quasi-1D motion of the tetramer takes place by a zigzag sequence of short-diagonal glide jumps in order to avoid the obstacles represented by the substrate atoms.

The existence of the different individual diffusion mechanisms described in this work, with their particular activation energies and prefactors, offers the possibility to manipulate the degree of diffusion anisotropy of these islands by adequately controlling the temperature. For instance, we estimate that at 135 K, the probability of a shear rotation event is only 1% with respect to that of the short-diagonal jumps; the other rotation mechanisms are much less likely. Diffusion anisotropy plays an important role in epitaxial growth [15,49,68] and for the fabrication of artificial nanostructures. Although in practice the selection of atomic clusters of a single size is unfeasible, the general phenomena and concepts presented in this paper might also be applicable to other objects, such as molecules. Detailed numerical simulation studies of the diffusion mechanisms of relatively complex molecules are affordable nowadays and the

information derived from them can be useful to design efficient strategies for the obtention of specific structures.

### V. SUMMARY

The surface diffusion of compact Cu tetramers on Cu(111) has been studied by molecular dynamics simulations using EAM interatomic potentials. Several different atomic-scale jump mechanisms are observed; from an Arrhenius analysis of the different occurrence frequencies over a broad temperature range, we have determined their individual activation energies and prefactors. It is found that the most abundant diffusion events are the concerted glides that transfer the tetramer between nearby fcc and hcp adsorption sites aligned closest to the cluster's short diagonal. Glide jumps parallel to the tetramer's long axis only take place at elevated temperatures; the low value of their prefactor suggests that this mechanism requires a high degree of atomic correlations to occur. Furthermore, the analysis of the cluster shape during both types of jumps indicates that they are fundamentally different processes, although their activation energies are similar. Several different rotation mechanisms have also been identified.

Our analysis of the diffusion coefficients derived from the mean-squared path covered by the tetramer as a function of time and temperature reveals that the cluster's long-distance motion is dominated by the linear glide mechanisms, since they produce the largest displacement of its center of mass. Their very different prefactors result in quasi-one-dimensional diffusion at low temperature, with a crossover to standard, two-dimensional motion at high temperatures as the rotational jumps with their higher activation energies are gradually activated and allow the tetramer to change its orientation over the surface.

### ACKNOWLEDGMENTS

This work has been financially supported in Spain by the MCyT through Grant No. FIS2010-18531, in Argentina by Grant No. PICT 0294/2010 Raíces, and by the UNL through Grant No. CAI+D 6-6-62. The authors also gratefully acknowledge the "Centro de Computación Científica" (CCC) of the UAM for providing computing time through the *Moldy* project.

- 
- [1] T. T. Tsong, *Rep. Prog. Phys.* **51**, 759 (1988).
  - [2] M. C. Tringides, *Surface Diffusion: Atomistic and Collective Processes* (Springer, New York, 1997).
  - [3] Z. Zhang and M. G. Lagally, *Science* **276**, 377 (1997).
  - [4] G. de Lorenzi and G. Jacucci, *Surf. Sci.* **164**, 526 (1985).
  - [5] G. L. Kellogg, *Phys. Rev. Lett.* **73**, 1833 (1994).
  - [6] C. Chen and T. T. Tsong, *Phys. Rev. Lett.* **64**, 3147 (1990).
  - [7] J. C. Tully, G. H. Gilmer, and M. Shugard, *J. Chem. Phys.* **71**, 1630 (1979).
  - [8] G. de Lorenzi, G. Jacucci, and V. Pontikis, *Surf. Sci.* **116**, 391 (1982).
  - [9] S. C. Wang, J. D. Wrigley, and G. Ehrlich, *J. Chem. Phys.* **91**, 5087 (1989).
  - [10] J. Ferrón, R. Miranda, and J. J. de Miguel, *Phys. Rev. B* **79**, 245407 (2009).
  - [11] G. Antczak and G. Ehrlich, *Phys. Rev. B* **71**, 115422 (2005).
  - [12] M. S. Levine, A. A. Golovin, and V. A. Volpert, *Europhys. Lett.* **82**, 28007 (2008).
  - [13] J. Ferrón, L. Gómez, J. J. de Miguel, and R. Miranda, *Phys. Rev. Lett.* **93**, 166107 (2004).
  - [14] G. Antczak, *Phys. Rev. B* **74**, 153406 (2006).
  - [15] H. Brune, *Surf. Sci. Rep.* **31**, 125 (1998).
  - [16] H.-J. Freund, *Surf. Sci.* **500**, 271 (2002).
  - [17] C. M. Chang, C. M. Wei, and S. P. Chen, *Phys. Rev. Lett.* **85**, 1044 (2000).
  - [18] G. L. Kellogg and A. F. Voter, *Phys. Rev. Lett.* **67**, 622 (1991).
  - [19] D. W. Bassett, *Surface Mobilities on Solid Materials* (Plenum, New York, 1983).
  - [20] J. W. Evans, P. A. Thiel, and M. C. Bartelt, *Surf. Sci. Rep.* **61**, 1 (2006).
  - [21] Y. A. Kryukov and J. G. Amar, *Phys. Rev. E* **83**, 041611 (2011).
  - [22] J. Yang, W. Hu, J. Tang, and M. Xu, *J. Phys. Chem. C* **112**, 2074 (2008).
  - [23] G. L. Kellogg, T. T. Tsong, and P. Cowan, *Surf. Sci.* **70**, 485 (1978).
  - [24] S. C. Wang and G. Ehrlich, *Surf. Sci.* **239**, 301 (1990).
  - [25] G. L. Kellogg, *Appl. Surf. Sci.* **67**, 134 (1993).
  - [26] G. Antczak and G. Ehrlich, *Surf. Sci. Rep.* **62**, 39 (2007).
  - [27] M. S. Daw and M. I. Baskes, *Phys. Rev. Lett.* **50**, 1285 (1983).
  - [28] S. M. Foiles, M. I. Baskes, and M. S. Daw, *Phys. Rev. B* **33**, 7983 (1986).
  - [29] A. F. Voter and S. P. Chen, *Proceedings of the Characterization of Defects in Materials, Boston, 1986* (Materials Research Society, Pittsburgh, 1987).
  - [30] D. W. Bassett, *J. Phys. C: Solid State Phys.* **9**, 2491 (1976).
  - [31] A. F. Voter, *Phys. Rev. B* **34**, 6819 (1986).
  - [32] C.-L. Liu and J. B. Adams, *Surf. Sci.* **268**, 73 (1992).
  - [33] J. C. Hamilton, M. S. Daw, and S. M. Foiles, *Phys. Rev. Lett.* **74**, 2760 (1995).
  - [34] A. G. Naumovets and Z. Zhang, *Surf. Sci.* **500**, 414 (2002).
  - [35] M. Müller, K. Albe, C. Busse, A. Thoma, and T. Michely, *Phys. Rev. B* **71**, 075407 (2005).
  - [36] P. Salo, J. Hirvonen, I. T. Koponen, O. S. Trushin, J. Heinonen, and T. Ala-Nissila, *Phys. Rev. B* **64**, 161405 (2001).
  - [37] A. Bogicevic, S. Liu, J. Jacobsen, B. Lundqvist, and H. Metiu, *Phys. Rev. B* **57**, R9459 (1998).
  - [38] A. Karim, A. Kara, O. Trushin, and T. S. Rahman, *J. Phys.: Condens. Mater.* **23**, 462201 (2011).
  - [39] K. Kyuno and G. Ehrlich, *Surf. Sci.* **437**, 29 (1999).
  - [40] A. Karim, A. N. Al-Rawi, A. Kara, T. S. Rahman, O. Trushin, and T. Ala-Nissila, *Phys. Rev. B* **73**, 165411 (2006).
  - [41] O. U. Uche, D. Perez, A. F. Voter, and J. C. Hamilton, *Phys. Rev. Lett.* **103**, 046101 (2009).
  - [42] S. I. Shah, G. Nandipati, A. Kara, and T. S. Rahman, *Phys. Rev. B* **88**, 035414 (2013).

- [43] C. Ghosh, A. Kara, and T. S. Rahman, *Surf. Sci.* **601**, 3159 (2007).
- [44] C.-L. Liu, *Surf. Sci.* **316**, 294 (1994).
- [45] J. C. Flores, B. H. Aguilar, A. M. Coronado, and H. Huang, *Surf. Sci.* **601**, 931 (2007).
- [46] J. Heinonen, I. Koponen, J. Merikoski, and T. Ala-Nissila, *Phys. Rev. Lett.* **82**, 2733 (1999).
- [47] A. W. Signor, H. H. Wu, and D. R. Trinkle, *Surf. Sci.* **604**, L67 (2010).
- [48] J. C. Hamilton, *Phys. Rev. Lett.* **77**, 885 (1996).
- [49] M. G. Lagally, *Phys. Today* **46**, 24 (1993).
- [50] Z.-P. Shi, Z. Zhang, A. K. Swan, and J. F. Wendelken, *Phys. Rev. Lett.* **76**, 4927 (1996).
- [51] J. R. Sanchez and J. W. Evans, *Phys. Rev. B* **59**, 3224 (1999).
- [52] R. Ferrando and A. Fortunelli, *J. Phys.: Condens. Matter* **21**, 264001 (2009).
- [53] M.-C. Marinica, C. Barreateau, M. C. Desjonquères, and D. Spanjaard, *Phys. Rev. B* **70**, 075415 (2004).
- [54] M. Breeman, G. T. Barkema, and D. O. Boerma, *Surf. Sci.* **323**, 71 (1995).
- [55] J. Rifkin, <http://www.ims.uconn.edu/centers/simul/> (unpublished).
- [56] R. A. Johnson, *Phys. Rev. B* **37**, 3924 (1988).
- [57] See Supplemental Material at <http://link.aps.org/supplemental/10.1103/PhysRevB.90.125437> for sample movies at several temperatures displaying all the different cluster motion mechanisms described in the text.
- [58] R. M. Nicklow, G. Gilat, H. G. Smith, L. J. Raubenheimer, and M. K. Wilkinson, *Phys. Rev.* **164**, 922 (1967).
- [59] G. Treglia and M.-C. Desjonquères, *J. Phys. France* **46**, 987 (1985).
- [60] U. Kürpick and T. S. Rahman, *Surf. Sci.* **383**, 137 (1997).
- [61] G. G. Kallinteris, G. A. Evangelakis, and N. I. Papanicolaou, *Surf. Sci.* **369**, 185 (1996).
- [62] U. Kürpick, *Phys. Rev. B* **64**, 075418 (2001).
- [63] J. Repp, F. Moresco, G. Meyer, K. H. Rieder, P. Hylgaard, and M. Persson, *Phys. Rev. Lett.* **85**, 2981 (2000).
- [64] N. Knorr, H. Brune, M. Epple, A. Hirstein, M. A. Schneider, and K. Kern, *Phys. Rev. B* **65**, 115420 (2002).
- [65] V. Chirita, E. P. Münger, J. E. Greene, and J.-E. Sundgren, *Surf. Sci.* **436**, L641 (1999).
- [66] O. S. Trushin, P. Salo, and T. Ala-Nissila, *Phys. Rev. B* **62**, 1611 (2000).
- [67] W. Meyer and H. Neldel, *Z. Tech. Phys. (Leipzig)* **18**, 588 (1937).
- [68] T. Ala-Nissila and S. C. Ying, *Prog. Surf. Sci.* **39**, 227 (1992).